ADVANCED ELECTRONIC MATERIALS
www.advelectronicmat.de

Bioinspired Metal Mesh Structure with Significant Electrical and Optical Properties

Neha Sepat, Vikas Sharma, Satyavir Singh, and Kanupriya Sachdev**

1D metal network is one of the promising alternatives of the conventional transparent conducting electrode (TCE) viz ITO/FTO. Bioinspired fabrication of junction resistance free metal grid structures is explored for their TCE applications. The leaf-based metal grid electrodes exhibit low DC resistivity (10^{-5}–10^{-4} Ω cm) and high optical transparency (80–90%) in the visible spectrum. The leaf vein structures are varied to obtain better optoelectronic properties. Finally, a multilayered stacked structure (SnO_2-Ag-Au-SnO_2) is deposited on a poly ethyl terephthalate substrate and low- to high-temperature electrical stability is demonstrated. X-ray photoelectron spectroscopy results are used to investigate the structural study of the leaf-based 1D structure. A minimal variation in R_s values is seen even after 1000 times bending for the flexible transparent structure. It is demonstrated that the specific leaf vein–based metal structures can attain good optical, electrical, and mechanical performance.

1. Introduction

The transparent conducting electrode is one of the most prominent components of optoelectronic devices, having a direct effect on device performance.[1,2] Solar cells,[3] smart windows,[4] light emitting diodes,[5] water splitting devices,[6] etc. require at least one transparent and conducting electrode in the structure. Indium tin oxide (ITO) and fluorine tin oxide (FTO) the most conventional materials have some associated problems like scarcity, high deposition cost, less flexibility, and toxicity.[7] More new applications such as smart windows, transparent heaters, and transparent sensors are emerging day by day.[8,9] Considering both, the demand for high-performance TCE and associated problems with the conventional transparent electrode, the need for the search of an alternative to ITO has become very high.[10] Various indium-free transparent electrode materials have been investigated, such as metal nanowire networks,[11] silver nanowire (Ag NW) films,[12] metallic grids,[13] conjugated polymers/ conducting polymers,[14] carbon nanotubes (CNTs),[15] hybrid CNT-Ag structure,[16] graphene,[17] several conducting oxides Ga:ZnO, Al:ZnO,[18] etc. Macroscopic metal grids have been successfully developed and used as a front electrode for inorganic solar cells and are a potential replacement of thin metal films as transparent electrode (TE) in organic optoelectronic devices also.[19] They exhibit high visible light transparency due to the large open area between the thick lines of metals and high conductivity due to the continuity of mesh with metal lines crossing each other and reduced junction resistance. Tuning of the work function is also possible by selecting the metal.[20] Photolithography, nanolithography, or transfer printing methods have been employed to develop metal grid electrodes, which however are complicated and tedious processes.[21,22] Metal nanowires–based 1D network shows the high merit of optical and electrical properties on becoming an excellent transparent conducting electrode, but suffer from certain limitations such as rough surface finish, poor adhesion properties, change in properties with temperature variation. The bare Ag NW suffers from oxidation and melting issues when exposed to temperature and air during device fabrication and application. The best possible solution is to cover such a structure with high refractive index n-type materials with high thermal stability. The metal oxide is a suitable candidate to combine with such nanostructures. Hybrid structures (dielectric/metal NW/dielectric, DMD) have been used to resolve these issues.[3] Here, metal governs the electrical while dielectric layer improves optical properties of the hybrid structure.[23] This conventional DMD structure possesses adequate transparency in the visible region. These DMD structures due to high transparency and sufficient conductivity show great promise for their potential use in next-generation optoelectronic and energy devices.[24] Metal mesh is preferred over nanowires/macrowires because of less contact and junction resistance.[25] There are few reports of fabrication of metal nanostructure using soft lithography[9] and leaf structure[25] for energy and optoelectronics applications.[26] However, an extensive investigation is needed to test the structural properties and stability over a wide temperature range of such structures.

The present research work reports the fabrication and study of bioinspired metal grid electrode. The electrode exhibits better,

N. Sepat, Dr. V. Sharma, S. Singh, Prof. K. Sachdev
Department of Physics
Malaviya National Institute of Technology Jaipur
Jaipur 302017, India
E-mail: phyvikas@gmail.com; ksachdev.phy@mnit.ac.in
Dr. V. Sharma
Department of Physics
Indian Institute of Technology Delhi
New Delhi 110016, India
Prof. K. Sachdev
Materials Research Center
Malaviya National Institute of Technology Jaipur
Jaipur 302017, India

DOI: 10.1002/aelm.201800318

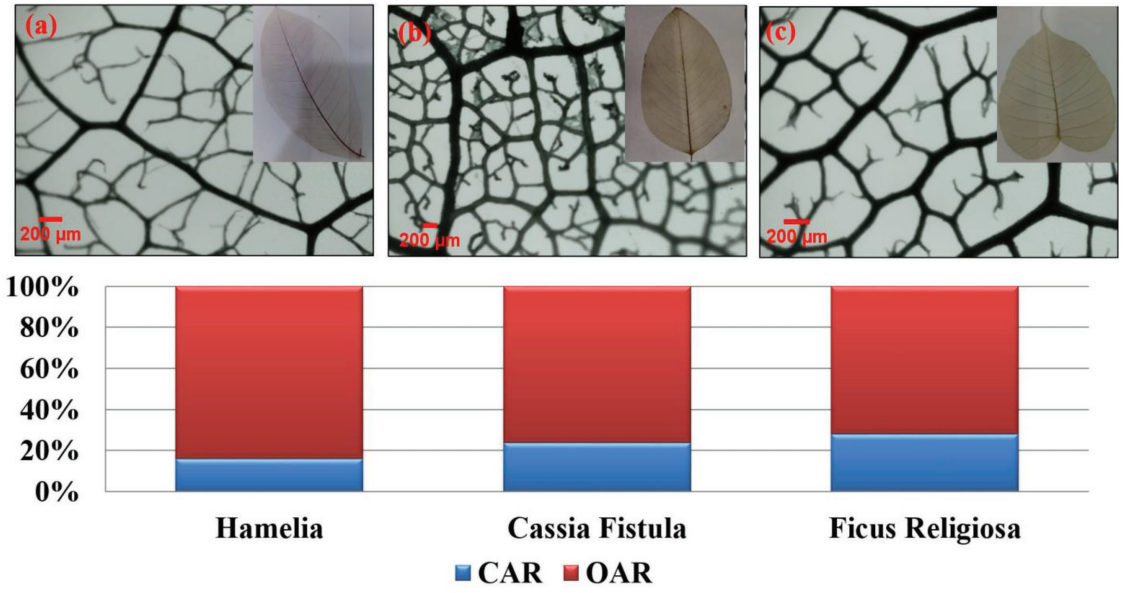

Figure 1. Corresponding images showing the optical images of etched a) Hamelia b) Cassia fistula, and c) Ficus Religiosa leaves. The lower part shows the area fraction of the OAR to the CAR for Hamelia, Cassia fistula, and Ficus Religiosa.

or similar electrical conductivity and optical transparency in the visible spectrum as compared to ITO coated substrate. The oppositely paired veins provide high conductivity and the open area between veins bring high transparency. The leaf vein structures are varied using different leaves to obtain better optoelectronic properties. The metal grids are produced using Au, Ag, and Ag-Au metals for single layered and double layered metal grids, respectively. These metal grids are embedded between two tin oxide layers to get the final multilayer stacked structure.

2. Result and Discussion

The leaves have a vein structure which can be used as a template for fabrication of metal grid. The process used to get the vein structure to be used as a template for fabrication of metal mesh is given in Supporting Information. Three different leaves (Hamelia, Ficus Religiosa, and Cassia fistula) were used as templates for metal grid fabrication. **Figure 1**, gives the optical images of particular leaf templates. The optical measurements show (Figures S2–S4, Supporting Information) that Hamelia leaf is the best template for metal mesh fabrication.

The covered area ratio (CAR) for all three leaf vein structure is shown in the lower part of Figure 1. It denotes the fraction of the area occupied by metal vein, whereas the open area ratio (OAR) represents the unoccupied fraction. OAR and CAR percentages were analyzed using water shading tool of ImageJ. OAR for Hamelia, Cassia fistula, and Ficus Religiosa was 84%, 76% and 72%, respectively. Hamelia leaf has maximum OAR 84% giving highest transmittance in comparison to Cassia fistula and Ficus Religiosa leaves and hence was chosen as a template. The OAR and CAR do not directly calculate or represent the distribution or density of the mesh structure; these are used to relate the optical and electrical behavior of such a mesh structure.

The metal mesh (Ag, Au, and a bilayer of Ag-Au) was deposited on the etched vein structure of leaf and transferred to a flexible poly ethyl terephthalate (PET) sheet for further study. A schematic diagram of the process is given in **Figure 2**. The use of Ag in energy and optoelectronic devices faces some problems in terms of oxidation and melting with exposure to temperature and air.[3] To protect the bare silver we used the gold as a protective layer. Gold is highly stable regarding temperature and is a good conductor also.[27]

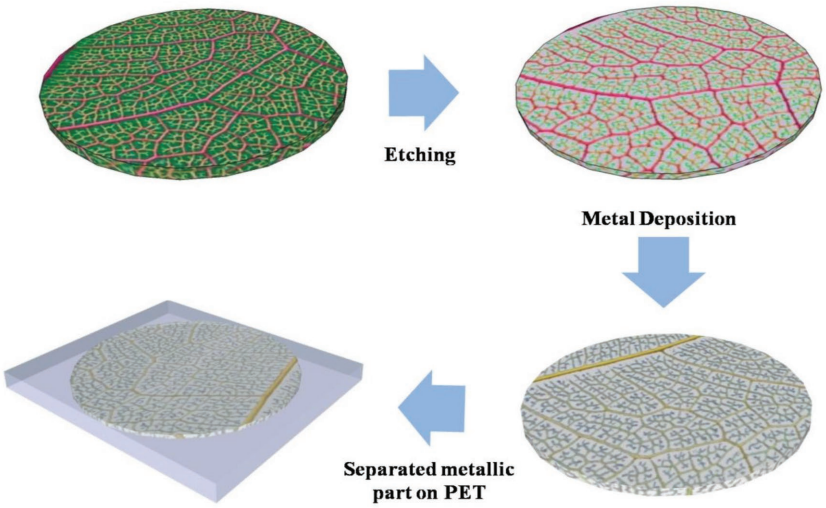

Figure 2. Schematic description of vein structure–based metal mesh fabrication process on PET.

2.1. Structural Study

X-ray diffraction (XRD) pattern of the SnO_2-Ag-Au-SnO_2 composite sample is shown in **Figure 3**. Diffraction peaks at $2\theta = 38.144°$, 44.3788°, 64.5485°, and 77.5335° are due to reflection from (111), (200), (220), and (311) planes of Ag (JCPDS No. 04-0783), respectively. The peak positions for the Au (JCPDS No. 04-0784) at $2\theta = 38.144°$, 44.3788°, 64.5485°, and 77.5335° are assigned to the (111), (200), (220), and (311) planes.[28] The high-intensity Ag peak in XRD of SnO_2-Ag-Au-SnO_2 structure was observed due to the annealing effect.[29] After silver deposition, the Ag vein structure was heated beneath to remove the vein part of the specimen. No peak is seen for SnO_2 showing amorphous behavior which is due to deposition being done at room temperature.[24] Amorphous behavior will also support the flexibility of the hybrid multilayer structure.

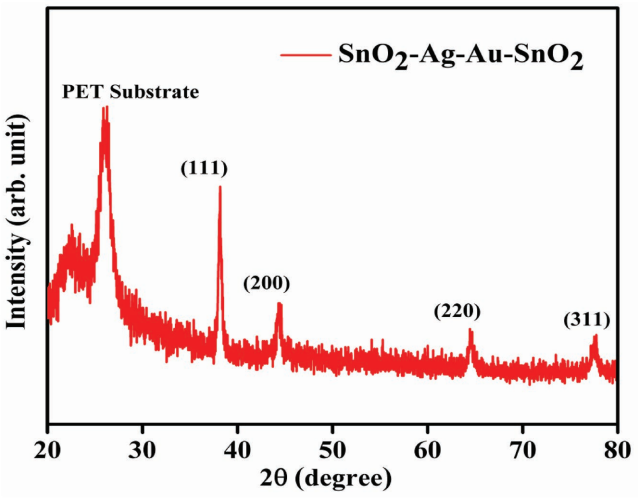

Figure 3. XRD pattern of the SnO_2-Ag-Au-SnO_2 composite sample on PET substrate.

2.2. Surface characterization

Scanning electron microscope (SEM) images (**Figure 4**) show the metal following the morphology and structure of the vein.[25] Minimum and a maximum thickness of 10 and 130 µm, respectively is seen for Hamelia leaf veins. The leaf has interconnected veins with minimum free ends in comparison to the other two leaves. Compared to that, the minimum and maximum thickness for Cassia fistula leaf is 10 and 80 µm,

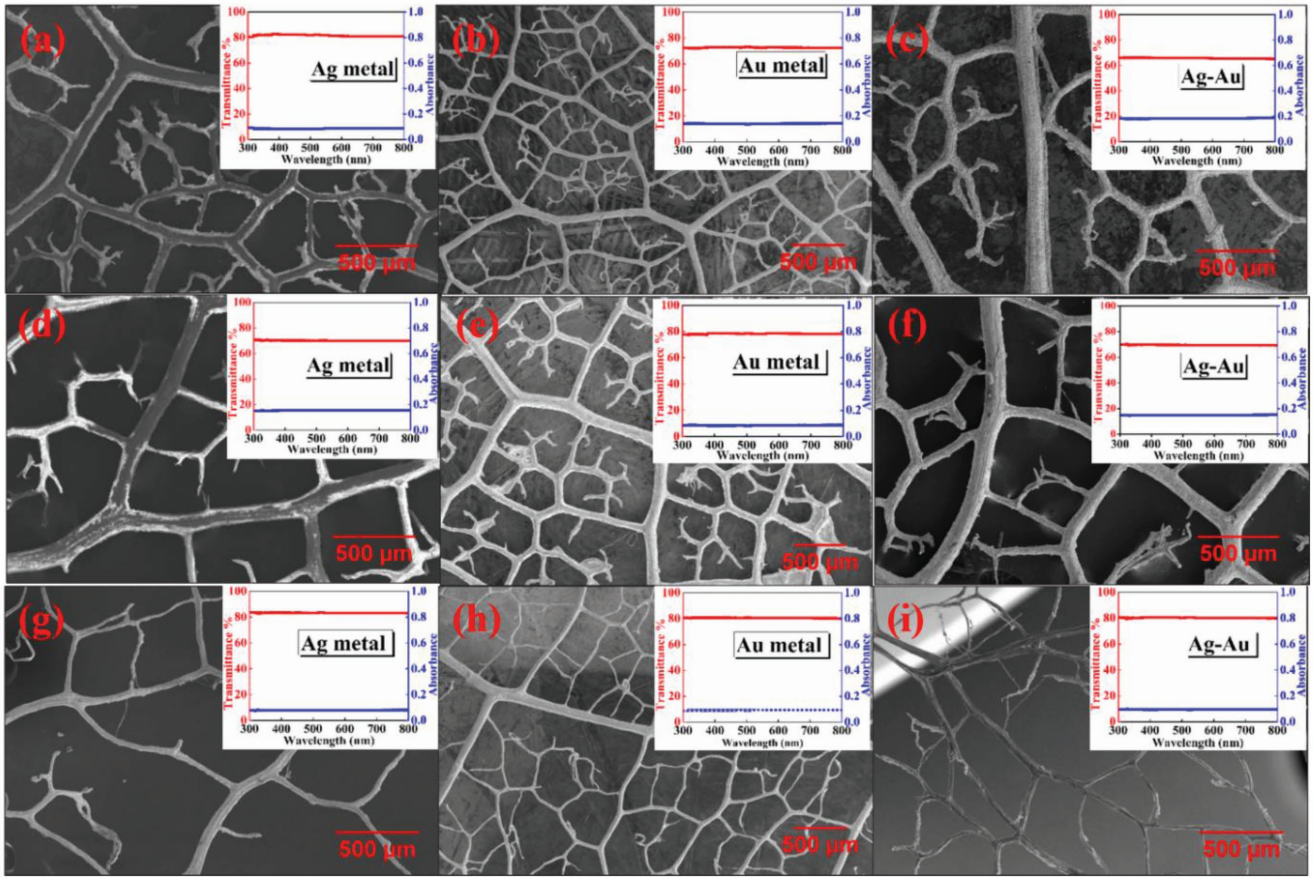

Figure 4. SEM images of metal mesh a) Ag using Cassia Fistula, b) Au using Cassia Fistula, c) Ag-Au using Cassia Fistula, d) Ag using Ficus Religiosa, e) Au using Ficus Religiosa, f) Ag-Au using Ficus Religiosa, g) Ag using Hamelia, h) Au using Hamelia, i) Ag-Au using Hamelia leaf vein structures and inset graphs show the transmittance and absorbance of the respective metal mesh.

respectively. The Ficus Religiosa leaf has thick and free end wires with a maximum thickness of 150 µm and a minimum thickness of 40 µm. The gold-coated Hamelia leaf structure is shown in Figure S7 in the Supporting Information. The SEM images of SnO_2-Au-Ag-SnO_2 composite on PET are given in Figure S8 in the Supporting Information. The maximum and minimum thickness of the mesh wire is ≈52 and 2 µm, respectively, analyzed using ImageJ. The morphology of joint of wires is shown in Figure S8 in the Supporting Information.

2.3. Optical Properties

The optical transmittance recorded with UV–vis spectrometer is above 80% for all metal meshes fabricated using Hamelia leaves vein structure (comparison available in Supporting Information) and less than 80% for the metal mesh structure fabricated using the other two leaves. The possible reason for the difference in transmittance is the difference in open area percentage of different leaf vein structure as Hamelia leaf has the maximum open area.

The optical properties of the composite specimen are crucial and depend on the OAR of the metal mesh and reflections caused by it. The primary work of the oxide layer in the composite specimen is to increase the transparency in the visible region by decreasing the reflections from the metal mesh surface. The overall transmittance depends on the reflection losses and it can be boosted by adding oxide layers on both sides of the middle layers.

The prepared metal grid was then embedded between two metal oxide layers as a SnO_2-Au-Ag-SnO_2 composite. The optical properties of the multilayer composite are presented in **Figure 5** exhibiting nearly constant values for transmittance beyond 450 nm of incoming radiation. Average transmittance for SnO_2-Au-Ag-SnO_2 composite in the range 350–2000 nm was measured to be 90.03%.In the visible region (350–800 nm) the multilayer showed 85.31% average transmittances. The reflectance spectra from the SnO_2-Au-Ag-SnO_2 structure are shown in Figure S5 in the Supporting Information.

The composite structure shows improved performance in transmittance as compared to that for bare metal grids because of less surface scattering of incident light. It is a well-known phenomenon that when the metal layer is embedded into a high refractive index material like dielectric or oxide with an appropriate thickness, it increases the transmittance due to less optical losses (mainly reduces the reflection from the metal surface).[23,3] There are many studies on dielectric/metal NW/dielectric (DMD) structure which conclude that T% was increased by adding an oxide layer.[30] SnO_2 is a well-known earth abundant wide bandgap material satisfying all the conditions to be used as a dielectric material in DMD structure. The bare metal mesh (Au-Ag) from Hamelia leaf template shows 80% transmittance in the visible resign and the transmittance enhances up to 84% when mesh structure is embedded into the SnO_2 layers (Figure S6, Supporting Information). Our previous investigations also suggest that transition metal oxides are best materials for such structures.[24,31]

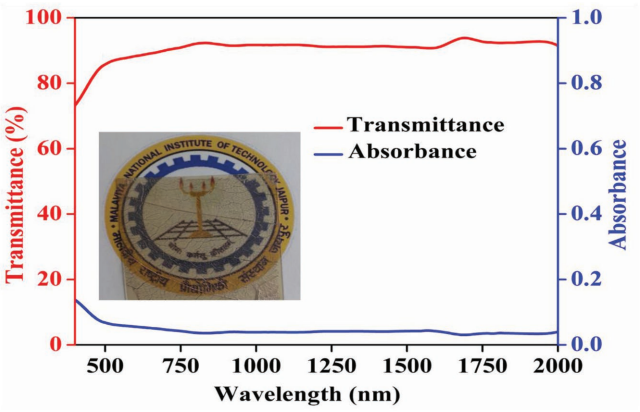

Figure 5. Transmittance and absorbance curves for SnO_2-Au-Ag-SnO_2 hybrid structure.

2.4. Electrical Measurement

The resistivity, carrier concentration, and mobility were determined using four point Hall measurement system. Table S1 in the Supporting Information gives the electrical transport property parameters for metal grids prepared using different leaf vein structures. The specimens are seen to have a high charge carrier density but limited mobility at room temperature. Metal grids using Hamelia leaves vein structure has a lower resistivity in comparison to that for the other two leaves. The DMD structure is the best combination to get high electrical conductivity and optical transmittance with minimum loss.[23] In a DMD, the embedded metal layer provides the electrical conductivity and the oxide layer enhances the optical property by reducing the reflectance.[31] SnO_2-Au-Ag-SnO_2 composite has the best resistivity 1.2×10^{-4} Ω cm, mobility 4.09 $cm^2\ V^{-1}\ s^{-1}$, and carrier concentration 1.2696×10^{22} cm^{-3} with the Au-Ag metal grid between SnO_2 layers fabricated using Hamelia leaf vein structure. The detailed charge transport mechanism is discussed in Figure S9 in the Supporting Information.[32] The proposed SnO_2-Au-Ag-SnO_2 composite structure behaves as a degenerate structure and full mechanism is yet to be understood.

We have also tested these samples using low-temperature Hall measurements to check the applicability of the prepared electrode in a wide range of temperature. These measurements were carried out using Van der Pauw configuration. The variation of resistivity for the temperature range of 80–340 K is presented in **Figure 6** for SnO_2-Au-Ag-SnO_2 composite using Hamelia leaf vein structure. The curve indicates that the resistivity for the composite sample is almost of the same order or behaves as a degenerate structure in the entire temperature range. Very high conductivity value is observed even at very low temperatures. The composite was shown to exhibit a resistivity value 1.5×10^{-4} Ω cm at 340 K, with a minimal variation up to 80 K.

The change in electrical resistivity with the carriers density and their mobility can be explained by the following expression

$$\rho = \frac{1}{n_e \mu e} \tag{1}$$

where ρ is resistivity, e is a charge on the electron, n_e is carrier density, and μ is the carrier mobility. The resultant resistance of

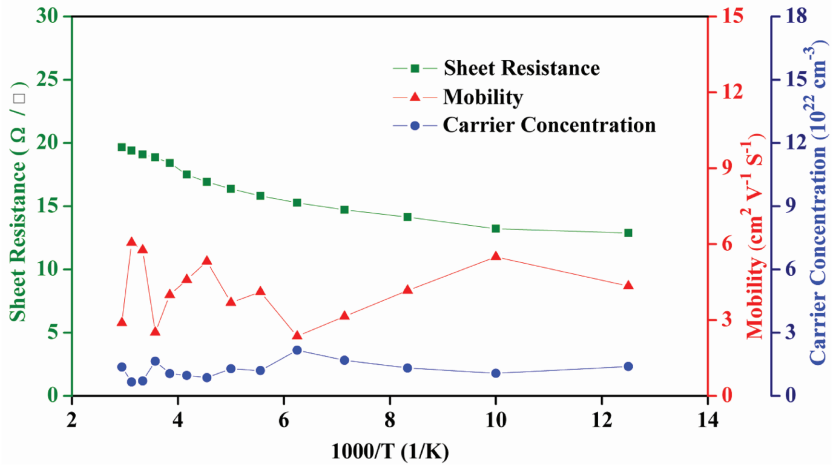

Figure 6. Sheet resistance, carrier concentration, and mobility as a function of reciprocal temperature for the SnO_2-Au-Ag-SnO_2 composite.

the composite specimen is usually explained by considering it a coplanar configuration and given by $1/R_{total} = 1/R_{metal} + 2/R_{oxide}$ with $R_{oxide} = 1000R_{metal}$ and hence $R_{total} = R_{metal}$. This indicates that the resistivity of the composite specimen is dominated by metal mesh only.

2.5. Mechanical Strength

The multilayer (SnO_2-Au-Ag-SnO_2) film showed excellent mechanical properties under the bending test where the film was repetitively bent at radius ≈4 mm. The resistivity of the film was measured after a certain number of bending cycles repetitively.[33] Resistivity values varied from 1.2×10^{-4} to 3.2×10^{-4} Ω cm till 1000 bending cycles as shown in **Figure 7**. The inset in Figure 7 shows a photograph of SnO_2-Au-Ag-SnO_2 film on a PET substrate, demonstrating its flexibility.

The SnO_2-Au-Ag-SnO_2 film maintained almost the same values of resistivity beyond 1000 bending cycles, whereas sheet resistance of the ITO film rises rapidly after 50 cycles.[34,35] Very high tolerance is seen for the SnO_2-Au-Ag-SnO_2 composite electrode to tensile stress in contrast to the ITO film and is attributable to the ductile metal mesh embedded in the metal oxide layers.

The leaf vein structure adopted by the metal mesh is the main reason for such mechanical strength. The vein structure of the leaves makes them highly flexible. So here, we used the same kind of structure geometry for our materials and measured the mechanical strength.[26,36] There are few reports on metal nanowires,[3] rods and grids,[37,22] and ultrathin films[38] which claim a similar kind of behavior regarding mechanical flexibility. The change in sheet resistance in metal mesh structure and ITO was plotted with respect to bending cycle and shown in Figure S10 in the Supporting Information.

2.6. XPS Investigation and FOM

X-ray photoelectron spectroscopy (XPS) was used for elemental analysis of metal grids. **Figure 8**a shows the high-resolution spectrum of gold metal mesh on Hamelia leaf structure. The sample was cleaned by Ar sputtering to remove the contaminants. The peaks positioned at 87.4 and 83.7 eV correspond to Au $4f_{5/2}$ and Au $4f_{7/2}$, respectively.[39] The binding energy difference between Au peaks is 3.6 eV, well matched with the reported results.[40] Figure 8b represents the Ag core level spectrum of the silver metal mesh on Hamelia leaf structure. The peaks positioned at 374 and 368 eV are corresponding to Ag $3d_{3/2}$ and Ag $3d_{5/2}$, respectively showing the valence state of Ag as 0.[40] Figure 8c,d represent the Ag 3d and Au 4f high-resolution spectrum of the Ag-Au metal mesh. The peaks positioned at 374.1 and 368.1 eV correspond to Ag $3d_{3/2}$ and Ag $3d_{5/2}$, respectively as shown in Figure 8c and peaks at 87.6 and 84 eV correspond to Au $4f_{5/2}$ and Au $4f_{7/2}$, respectively as shown in Figure 8d. The results are consistent with the standard binding energy of pure metal meaning thereby that the heat treatment while removing the metal mesh from the vein template has not caused a change in the valency of the bilayer electrode. The two peaks with binding energies of 495.2 eV for Sn $3d_{3/2}$ and 486.6 eV for Sn $3d_{5/2}$ in the core level spectrum (**Figure 9**) of Sn 3d[41] indicate the valance state of Sn as +4.[42]

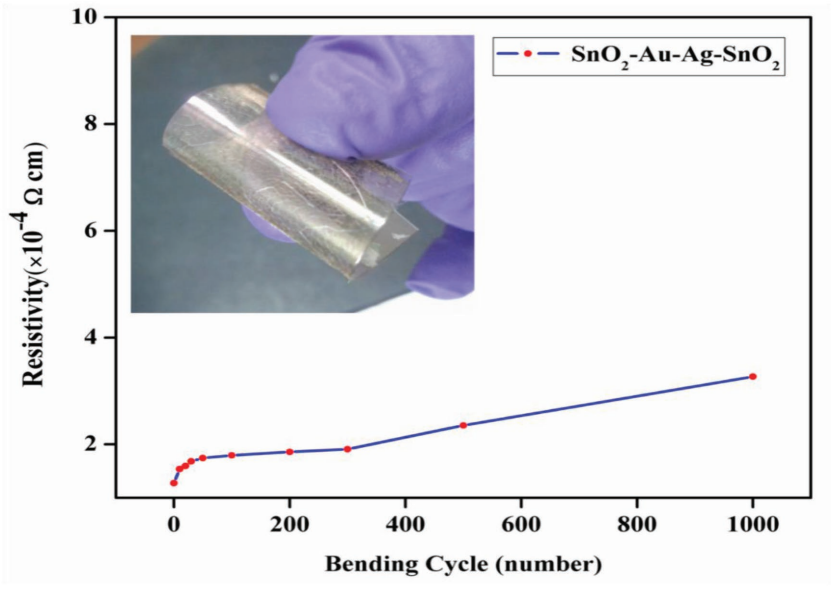

Figure 7. Variation of the resistivity during bend test for the SnO_2-Au-Ag-SnO_2composite on PET substrate and photograph of a flexible and transparent SnO_2-Au-Ag-SnO_2 composite electrode on a flexible polymer substrate PET.

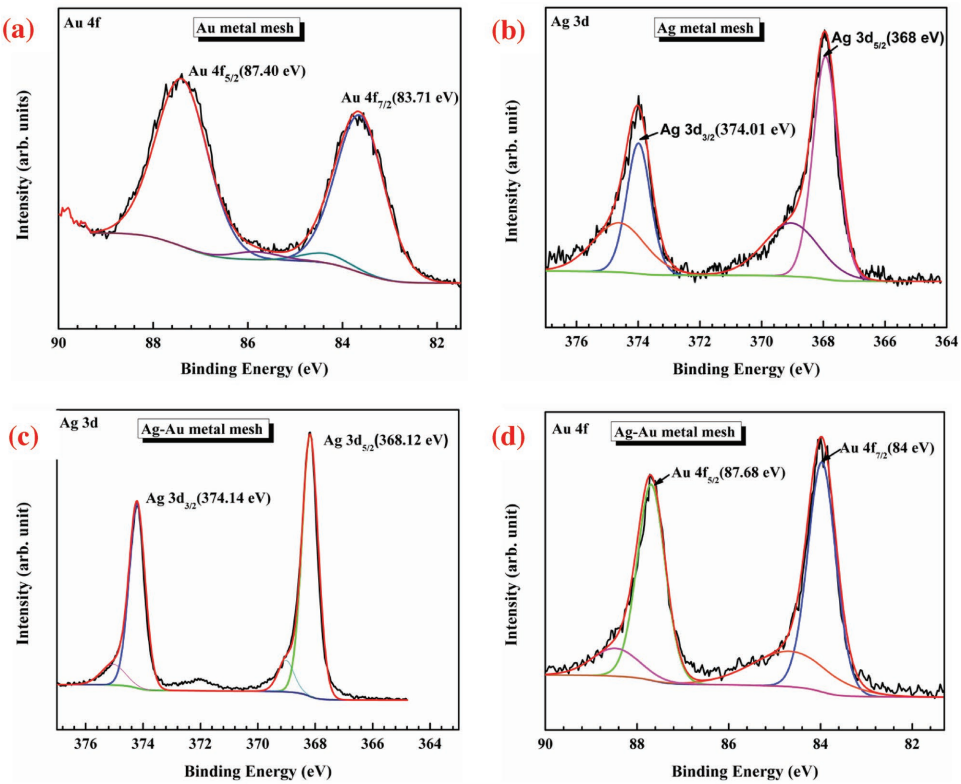

Figure 8. XPS spectra of a) Au 4f of Au, (b) Ag 3d of Ag, c) Ag 3d of Ag-Au, and d) Au 4f of Ag-Au Metal mesh having Hamelia vein structure.

Table 1 summarizes the optical and electrical properties of leaf vein–based metal mesh networks. It is useful to compare the performance of different metal meshes using the figure of merit (F_H) formula defined by Haacke as given by the relation[43]

$$F_H = \frac{T^{10}}{R_s} \tag{2}$$

where T is average transmission and R_s is the sheet resistance of the thin film. The calculated F_H are shown in Table 1. The composite structure is the most efficient electrode as it has the maximum figure of merit among all structures. A comparision in terms of figure of merit (FOM) between the different structures used for transparent electrode is presented in Table S2 in the Supporting Information.

3. Conclusion

A bioinspired fabrication approach is used to provide high-throughput and low-cost manufacturing of metal mesh for TCE applications. An excellent and interconnected vein structure template was produced by etching the green part of three

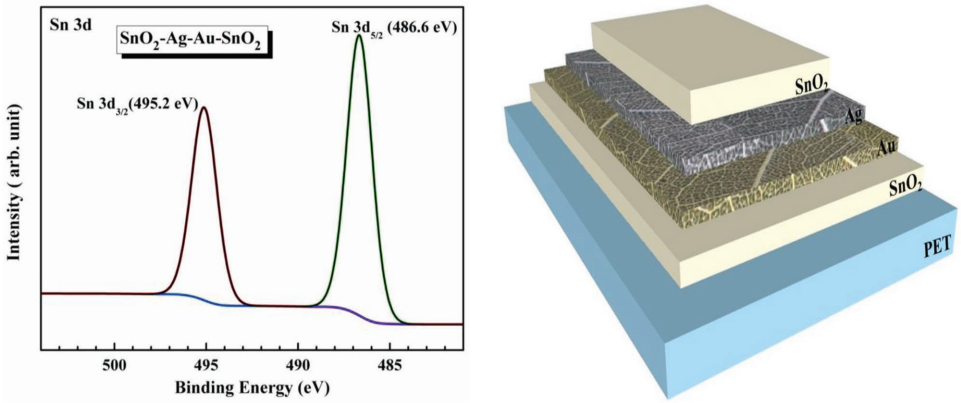

Figure 9. XPS spectra of SnO_2-Ag-Au-SnO_2composite having Hamelia vein structures and schematic structure of SnO_2-Au-Ag-SnO_2 hybrid structure.

Table 1. Sheet Resistance, transmittance, and figure of merit of the samples using Hamelia leaf vein structure.

	Au only metal-mesh	Ag only metal-mesh	Ag-Au metal-mesh	SnO_2-Ag-Au-SnO_2 metal-mesh
Sheet resistance [Ω/□]	17	12	14.7	15.02
Optical transmittance at 550 nm [%]	83.2	80.4	80.2	87.10
Average transmittance at 350–800 nm [%]	80.5	83.3	80.2	85.3
Figure of merit (F_H) [$\times 10^{-3}$]	6.7	13.3	7.4	13.6

types of leaves: Hamelia, Cassia Fistula, and Ficus Religiosa. Hamelia vein structure with largest OAR was the best template in comparison to the other two templates. All single and multilayered metal grids fabricated using Hamelia vein structure exhibited optical and electrical properties as good as to that of commercial substrates. When the Au-Ag metal grid was embedded between two SnO_2layers, the stability dramatically increased with slight increment in transparency. Negligible variation in resistivity values is measured after the composite is subjected to 1000 bending cycles and it is well known that the sheet resistance of the ITO films rises high after 50 cycles only. Hence the SnO_2-Au-Ag-SnO_2composite electrode shows excellent thermal and mechanical properties in addition to being highly conductive and transparent.

4. Experimental Section

Here two metals were used; gold and silver for the fabrication of mesh structure using natural leaves templates. The choice of the metals was due to a concern of oxidation and stability, and hence bilayer of Ag and Au was taken for transparent electrode application. Fresh leaves were immersed in 5 gm ml^{-1} Na_2CO_3 solution at 80 °C for varying periods depending on the vein thickness and roughness of the leaves. The green part in between veins was removed by a soft process followed by washing and drying and consequently, vein skeleton was obtained. The vein skeletons of leaves were pasted on glass substrates for metal deposition. The sputtering of the metal layer was done using a standard sputtering target at a vacuum of 10^{-3} mbar using SEM coater at room temperature. The deposition time was 120 s with a current 30 mA. Heat treatment method was used to separate the metallic mesh and transfer it to a flexible PET substrate. The thickness of the metal grid was ≈50 nm.

For the final stacked multilayer structure, tin oxide of 30 nm was coated on a clean, flexible PET substrate by RF sputtering. The metal mesh structure was transferred to the SnO_2-coated PET and finally, upper 30 nm SnO_2 layer was again coated using RF sputtering to get a hybrid structure which exhibited high optical transmittance and high electrical conductivity. A schematic diagram of the process is given in Figure 2. Moreover, a schematic structure of SnO_2-Ag-Au-SnO_2 composites is given in Figures 2 and 9. The fabricated structure was characterized by FEI Nova Nano 450 field emission scanning electron microscope (FESEM) for its morphological investigation. Perkin Elmer LAMBDA 750 UV–vis spectroscopy was used to measure the optical properties of the leaf template–based hybrid structure. Hall measurements at room temperature and with variation in temperature (80—350 K) were done by Ecopia 5500 Hall measurement system by four point probe method. Detailed investigation of the chemical state of elements was carried out by XPS (Omicron ESCA). Monochromatic source Al Kα (1486.7 eV) with 124 mm mean radius and X-ray resolution of 0.6 eV and 3×10^{-10} mbar chamber pressure were used for XPS measurement.

Supporting Information

Supporting Information is available from the Wiley Online Library or from the author.

Acknowledgements

Authors thank the Materials Research Centre, MNITJ for providing characterization facilities for this work.

Conflict of Interest

The authors declare no conflict of interest.

Keywords

Hall measurements, leaf veins, metal meshes, transparent conducting electrodes, X-ray photoelectron spectroscopy (XPS)

Received: May 18, 2018
Revised: July 19, 2018
Published online: November 12, 2018

[1] K. Ellmer, *Nat. Photonics* **2012**, *6*, 809.
[2] H. Ohta, H. Hosono, *Mater. Today* **2004**, *7*, 42.
[3] A. Kim, Y. Won, K. Woo, C.-H. Kim, J. Moon, *ACS Nano* **2013**, *7*, 1081.
[4] X. Bai, S. Lin, H. Wang, Y. Zong, H. Wang, Z. Huang, D. Li, C. Wang, H. Wu, *npj Flexible Electron.* **2018**, *2*, 3.
[5] H. Yoon, D. S. Shin, B. Babu, T. G. Kim, K. M. Song, J. Park, *Mater. Des.* **2017**, *132*, 66.
[6] H. Luo, Z. Fang, N. Song, T. Garvey, R. Lopez, T. J. Meyer, *ACS Appl. Mater. Interfaces* **2015**, *7*, 25121.
[7] C. J. M. Emmott, A. Urbina, J. Nelson, *Sol. Energy Mater. Sol. Cells* **2012**, *97*, 14.
[8] Z. Q. Zheng, J. D. Yao, B. Wang, G. W. Yang, *Sci. Rep.* **2015**, *5*, 11070.
[9] G. U. Kulkarni, S. Kiruthika, R. Gupta, K. Rao, *Curr. Opin. Chem. Eng.* **2015**, *8*, 60.
[10] A. Kumar, C. Zhou, *ACS Nano* **2010**, *4*, 11.
[11] M. E. Layani-Tzadka, E. Tirosh, G. Markovich, *ACS Omega* **2017**, *2*, 7584.
[12] W. W. He, X. H. Yan, Y. M. Liang, Y. F. Long, C. Pan, J. L. Zhao, L. Chen, W. Xiong, Q. X. Liu, *RSC Adv.* **2018**, *8*, 12146.
[13] S. Choi, Y. Zhou, W. Haske, J. W. Shim, C. Fuentes-Hernandez, B. Kippelen, *Org. Electron.* **2015**, *17*, 349.
[14] E. C. Cho, C. P. Li, J. H. Huang, K. C. Lee, J. H. Huang, *ACS Appl. Mater. Interfaces* **2015**, *7*, 11668.
[15] Y. Zhou, R. Azumi, *Sci. Technol. Adv. Mater.* **2016**, *17*, 493.
[16] Surbhi, V. Sharma, S. Singh, P. Garg, K. Asokan, K. Sachdev, *Mater. Res. Express* **2018**, *5*, 025037.
[17] D. S. Hecht, L. Hu, G. Irvin, *Adv. Mater.* **2011**, *23*, 1482.
[18] D. S. Ghosh, T. L. Chen, N. Formica, J. Hwang, I. Bruder, V. Pruneri, *Sol. Energy Mater. Sol. Cells* **2012**, *107*, 338.

[19] B. R. Patil, M. Mirsafaei, P. P. Cielecki, A. L. F. Cauduro, J. Fiutowski, H. G. Rubahn, M. Madsen, *Nanotechnology* **2017**, *28*, 405303.
[20] M. T. Greiner, Z.-H. Lu, *NPG Asia Mater.* **2013**, *5*, e55.
[21] Y. Jin, Y. Cheng, D. Deng, C. Jiang, T. Qi, D. Yang, F. Xiao, *ACS Appl. Mater. Interfaces* **2014**, *6*, 1447.
[22] J. Park, K. Lee, H. D. Um, K. H. Kim, K. Seo, *Adv. Mater. Technol.* **2018**, *3*, 1.
[23] C. Guillén, J. Herrero, *Thin Solid Films* **2011**, *520*, 1.
[24] V. Sharma, R. Vyas, P. Bazylewski, G. S. Chang, K. Asokan, K. Sachdev, *RSC Adv.* **2016**, *6*, 29135.
[25] B. Han, Y. Huang, R. Li, Q. Peng, J. Luo, K. Pei, A. Herczynski, K. Kempa, Z. Ren, J. Gao, *Nat. Commun.* **2014**, *5*, 1.
[26] J. Gao, Z. Xian, G. Zhou, J. M. Liu, K. Kempa, *Adv. Funct. Mater.* **2017**, *28*, 1705023.
[27] T. Kim, A. Canlier, C. Cho, V. Rozyyev, J. Y. Lee, S. M. Han, *ACS Appl. Mater. Interfaces* **2014**, *6*, 13527.
[28] M. Girtan, *Sol. Energy Mater. Sol. Cells* **2012**, *100*, 153.
[29] L. Liu, S. Ma, H. Wu, B. Zhu, H. Yang, J. Tang, X. Zhao, *Mater. Lett.* **2015**, *149*, 43.
[30] A. Indluru, T. L. Alford, *J. Appl. Phys.* **2009**, *105*, 123528.
[31] V. Sharma, P. Kumar, A. Kumar, Surbhi, K. Asokan, K. Sachdev, *Sol. Energy Mater. Sol. Cells* **2017**, *169*, 122.
[32] H. Han, N. D. Theodore, T. L. Alford, *J. Appl. Phys.* **2008**, *103*, 013708.
[33] J. Choi, Y. S. Shim, C. H. Park, H. Hwang, J. H. Kwack, D. J. Lee, Y. W. Park, B. K. Ju, *Small* **2018**, *14*, 1.
[34] X. Chen, W. Guo, L. Xie, C. Wei, J. Zhuang, W. Su, Z. Cui, *ACS Appl. Mater. Interfaces* **2017**, *9*, 37048.
[35] B.-Y. Wang, E.-S. Lee, Y.-J. Oh, H. W. Kang, *RSC Adv.* **2017**, *7*, 52914.
[36] Z. Xian, B. Han, S. Li, C. Yang, S. Wu, X. Lu, X. Gao, M. Zeng, Q. Wang, P. Bai, M. J. Naughton, G. Zhou, J. M. Liu, K. Kempa, J. Gao, *Adv. Mater. Technol.* **2017**, *2*, 2.
[37] M. G. Kang, M. S. Kim, J. S. Kim, L. J. Guo, *Adv. Mater.* **2008**, *20*, 4408.
[38] Z. Xue, X. Liu, N. Zhang, H. Chen, X. Zheng, H. Wang, X. Guo, *ACS Appl. Mater. Interfaces* **2014**, *6*, 16403.
[39] K. Yu, Z. Wu, Q. Zhao, B. Li, Y. Xie, *J. Phys. Chem. C* **2008**, *112*, 2244.
[40] H. Chen, G. Liu, L. Wang, *Sci. Rep.* **2015**, *5*, 10852.
[41] S. Balachandran, K. Selvam, B. Babu, M. Swaminathan, *Dalton Trans.* **2013**, *42*, 16365.
[42] T. Nagata, O. Bierwagen, M. E. White, M. Y. Tsai, Y. Yamashita, H. Yoshikawa, N. Ohashi, K. Kobayashi, T. Chikyow, J. S. Speck, *Appl. Phys. Lett.* **2011**, *98,* 2.
[43] G. Haacke, *Ann. Rev. Mater. Sci.* **1977**, *7*, 73.

